The CMB bispectrum from bouncing cosmologies

JCAP11(2021)024, PCMD, Ruth Durrer, Nelson Pinto-Neto

Paola C. M. Delgado

Uniwersytet Jagielloński
Faculty of Physics, Astronomy and Applied Computer Science

UJ Particle Physics Phenomenology and Experiments Seminar, November 22, 2021

Outline

CMB quantities and non-gaussianity

- A very hot Universe, where protons and electrons are free; photons have a short mean free path due to Thomson scattering.
- Temperature decreases ($\sim 3000\mathrm{K}$): recombination; photons reach us.
- The last-scattering surface: radiates as a black body; microwaves nowadays; coming from every direction; $\Rightarrow$ CMB.

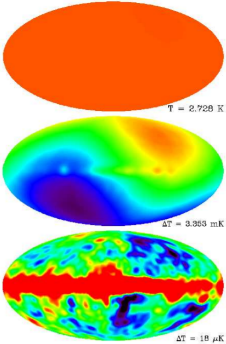

Figure 1: Figure from the COBE satellite (https://lambda.gsfc.nasa.gov/product/cobe/).

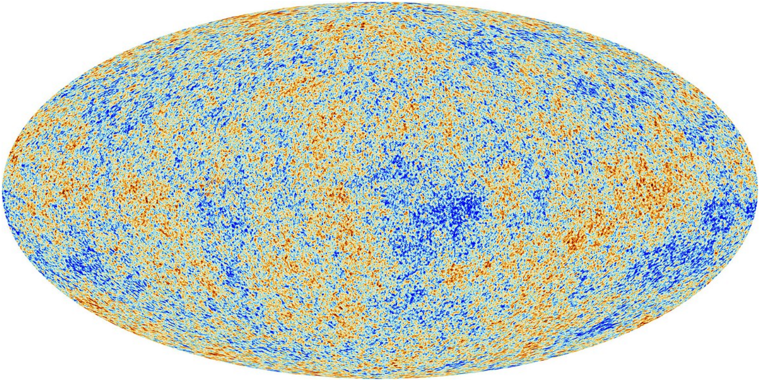

Figure 2: Figure from Planck 2018.

- The CMB temperature power spectrum: Sachs-Wolfe plateau at large scales (modes outside the horizon at recombination); peaks caused by acoustic oscillations for scales inside the horizon; Silk damping for smallest scales (recombination is not instantaneous and free path of photons is not zero).

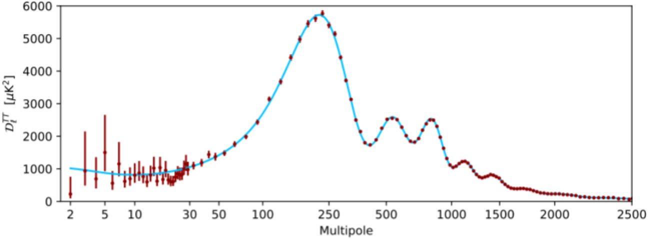

Figure 3: Figure from Planck 2018 (arXiv:1807.06205 [astro-ph.CO]).

- Temperature fluctuations:

$$\frac{\Delta T(\theta,\varphi)}{T_0} \equiv \sum_{\ell=2}^{\infty} \sum_{m=-\ell}^{\ell} a^T_{\ell m} Y_{\ell m}(\theta,\phi). \tag{1}$$

  $\ell = 1$ is highly contaminated by the kinetic dipole.
- CMB TT power spectrum:

$$\left\langle a^T_{\ell m} a^T_{\ell' m'} \right\rangle = C^{TT}_{\ell} \delta_{\ell\ell'} \delta_{mm'}. \tag{2}$$

- Observationally, we only have one sky. So we average over m:

$$\hat{C}_{\ell} = \frac{1}{2\ell+1} \sum_{m=-\ell}^{\ell} |a_{\ell m}|^2. \tag{3}$$

  When ℓ is small, we have cosmic variance.

- Gravity is non-linear. What about the 3-point correlation functions?

$$\langle X(\mathbf{k_1})X(\mathbf{k_2})X(\mathbf{k_3})\rangle = (2\pi)^3\delta(\mathbf{k_1}+\mathbf{k_2}+\mathbf{k_3})B_X(k_1,k_2,k_3), \quad (4)$$

  where B_X is the bispectrum.
- B is usually classified according to the triangle's shape for which it is maximal.

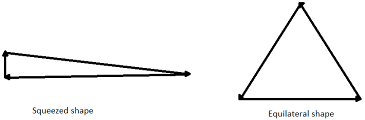

- Local non-Gaussianity:

$$\Psi(\mathbf{x}) = \Psi_G(\mathbf{x}) + f_{\rm nl}\left(\Psi_G^2(\mathbf{x}) - \left\langle \Psi_G^2 \right\rangle\right), \quad (5)$$

  where the Bardeen potential has a vanishing mean.
- Great reviews: Bartjan van Tent (arXiv:2017.10802v1 [astro-ph.CO]); Ruth Durrer, *The Cosmic Microwave Background*.

CMB anomalies at large scales & the lensing amplitude

- Large scale features that deviate from the ΛCDM predictions. p-values smaller than 1% to each anomaly.
- Power suppression: lack of 2-point correlations $C(\theta)$ for $\theta > 60^\circ$ (COBE, WMAP, Planck). The estimator of the total amount of correlations in $\theta > 60^\circ$, given by

$$S_{1/2} \equiv \int_{-1}^{1/2} [C(\theta)]^2 d(\cos\theta), \tag{6}$$

results in $S_{1/2} \approx 1500\mu K^4$. For ΛCDM: $45000\mu K^4$.

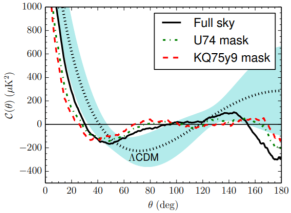

Figure 4: Figure from Craig J. Copi, Dragan Huterer, Dominik J. Schwarz, Glenn D. Starkman (arXiv:1310.3831 [astro-ph.CO]).

- Parity asymmetry: WMAP and Planck found an odd-parity preference. The estimator is given by

$$R^{TT}(\ell_{\max}) = \frac{D_+(\ell_{\max})}{D_-(\ell_{\max})}, \tag{7}$$

where $D_{+,-}(\ell_{\max})$ measures the power spectrum in even or odd multipoles, respectively, up to $\ell_{\max}$. ΛCDM predicts neutrality.

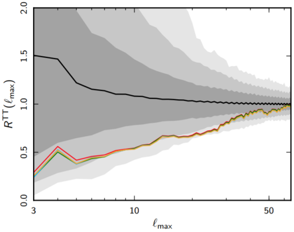

Figure 5: Figure from Planck 2015 (arXiv:1506.07135 [astro-ph.CO]).

- Dipolar asymmetry: can be seen in WMAP and Planck, only for large scales. Mathematically, this means a non-vanishing BipoSH coefficient $A^{1M}_{\ell,\ell+1}$. In terms of

$$A_1(\ell) \equiv \frac{3}{2}\sqrt{\frac{1}{3\pi}\sum_M |A^{1M}_{\ell,\ell+1}\mathscr{G}_\ell^{-1}|^2}, \tag{8}$$

  Planck finds $A_1 = 0.068 \pm 0.023$.
- The lensing amplitude A_L: introduced as a free parameter to provide a consistency test. $A_L = 1$ corresponds to the standard lensing in the Universe. The best-fit from Planck for ΛCDM is more than 2σ away from 1.
- Details on the anomalies can be found in I. Agullo, D. Kranas and V. Sreenath (arXiv:2006.09605v1 [astro-ph.CO]) and references therein.

A proposal to solve the anomalies

- Bounce preceding inflation, I. Agullo, D. Kranas, V. Sreenath (arXiv: 2005.01796 [astro-ph.CO]). Scale factor around the bounce:
$$a(t) = a_b(1 + bt^2)^n, \tag{9}$$
where $R_b = 12nb$.
- For $n = 1/6$ (LQC), the kinetic term is the largest just after the bounce. For larger n the potential is already relevant at the bounce.
- Initial quantum state is the adiabatic vacuum in the far past. At the onset of inflation, it deviates from Bunch-Davies.
- Non-Gaussianities arise, correlating super-horizon modes and infrared scales.

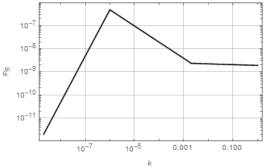

Figure 6: PCMD, R. Durrer, N. Pinto-Neto

- Non-Gaussianity increases the probability that some features appear in individual realizations of the primordial probability distribution.

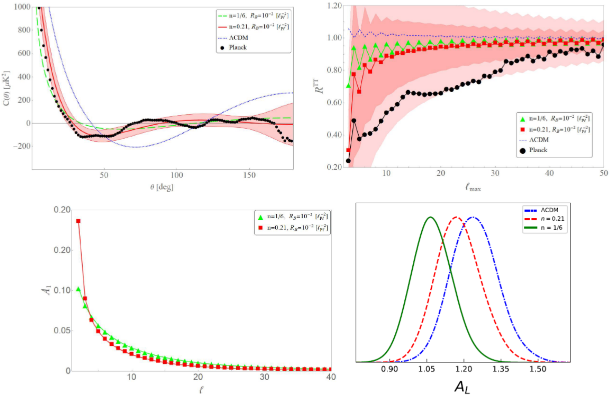

Figure 7: Figures from I. Agullo, D. Kranas, V. Sreenath (arXiv: 2005.01796 [astro-ph.CO])

- LQC and phenomenological model (best-fit):

n	γ	q	$f_{\rm nl}$ for $R_B = 1\ l_{Pl}^{-2}$	$f_{\rm nl}$ for $R_B = 10^{-3}\ l_{Pl}^{-2}$
$1/6$	0.6468	-0.7	3326	8518
0.21	0.751	-1.24	959	4372

- Power spectrum and bispectrum:

$$\mathscr{P}_{\mathscr{R}}(k) = A_s \begin{cases} (k/k_i)^2 (k_i/k_b)^q & \text{if } \ k \leq k_i \\ (k/k_b)^q & \text{if } \ k_i < k \leq k_b \\ (k/k_b)^{n_s - 1} & \text{if } \ k > k_b \,. \end{cases} \tag{10}$$

$$B(k_1, k_2, k_3) = \frac{3}{5}(2\pi^2)^2 f_{\rm nl} \left[\frac{\mathscr{P}_{\mathscr{R}}(k_1)}{k_1^3}\frac{\mathscr{P}_{\mathscr{R}}(k_2)}{k_2^3} + \frac{\mathscr{P}_{\mathscr{R}}(k_1)}{k_1^3}\frac{\mathscr{P}_{\mathscr{R}}(k_3)}{k_3^3} + \frac{\mathscr{P}_{\mathscr{R}}(k_3)}{k_3^3}\frac{\mathscr{P}_{\mathscr{R}}(k_2)}{k_2^3} \right] \times$$
$$\exp\left(-\gamma \frac{k_1 + k_2 + k_3}{k_b} \right) . \tag{11}$$

The bispectrum in the bounce+inflation model

- Recalling the definition of the bispectrum:

$$\frac{\Delta T}{T}(\mathbf{n}) = \sum_{\ell m} a_{\ell m} Y_{\ell m}(\mathbf{n}) \,, \tag{12}$$

$$\langle a_{\ell_1 m_1} a_{\ell_2 m_2} a_{\ell_2 m_3} \rangle = \mathscr{G}^{\ell_1 \ell_2 \ell_3}_{m_1 m_2 m_3} b_{\ell_1 \ell_2 \ell_3} = \begin{pmatrix} \ell_1 & \ell_2 & \ell_3 \\ m_1 & m_2 & m_3 \end{pmatrix} B_{\ell_1 \ell_2 \ell_3} \tag{13}$$

with

$$\mathscr{G}^{\ell_1 \ell_2 \ell_3}_{m_1 m_2 m_3} = \sqrt{\frac{\prod_{j=1}^{3}(2\ell_j + 1)}{4\pi}} \begin{pmatrix} \ell_1 & \ell_2 & \ell_3 \\ 0 & 0 & 0 \end{pmatrix} \begin{pmatrix} \ell_1 & \ell_2 & \ell_3 \\ m_1 & m_2 & m_3 \end{pmatrix} = g_{\ell_1 \ell_2 \ell_3} \begin{pmatrix} \ell_1 & \ell_2 & \ell_3 \\ m_1 & m_2 & m_3 \end{pmatrix} \tag{14}$$

- $b_{\ell_1 \ell_2 \ell_3}$ is the reduced bispectrum. It vanishes if the triangle inequality, $|\ell_1 - \ell_2| \leq \ell_3 \leq \ell_1 + \ell_2$, is not satisfied or if the sum $\ell_1 + \ell_2 + \ell_3$ is odd.

- Within linear perturbation theory,

$$b_{\ell_1\ell_2\ell_3} = \left(\frac{2}{\pi}\right)^3 \int_0^\infty dx\, x^2 \int_0^\infty dk_1 \int_0^\infty dk_2 \int_0^\infty dk_3 \times \left[\prod_{j=1}^{3} \mathscr{T}(k_j,\ell_j) j_{\ell_j}(k_j x)\right] (k_1 k_2 k_3)^2 B(k_1,k_2,k_3), \quad (15)$$

where, at large scales,

$$\mathscr{T}(k,\ell) \simeq \frac{1}{5} j_\ell(k(t_0 - t_{\mathrm{dec}}))\,. \quad (16)$$

- The bispectrum is separable in k-space:

$$(k_1 k_2 k_3)^2 B(k_1, k_2, k_3) = B_0 \left[f(k_1)f(k_2)g(k_3) + f(k_1)f(k_3)g(k_2) + f(k_3)f(k_2)g(k_1)\right] \tag{17}$$

$$B_0 = \frac{3}{5}(2\pi^2)^2 f_{\mathrm{nl}} \tag{18}$$

$$f(k) = \frac{\mathscr{P}_{\mathscr{R}}(k)}{k} \exp(-\gamma k/k_b) \tag{19}$$

$$g(k) = k^2 \exp(-\gamma k/k_b) \tag{20}$$

$$X_\ell(x, k) = \mathscr{T}(k, \ell) j_\ell(kx) f(k), \tag{21}$$

$$Z_\ell(x, k) = \mathscr{T}(k, \ell) j_\ell(kx) g(k), \tag{22}$$

$$X_\ell(x) = \int_0^\infty dk X_\ell(x, k), \tag{23}$$

$$Z_\ell(x) = \int_0^\infty dk Z_\ell(x, k), \tag{24}$$

$$b_{\ell_1 \ell_2 \ell_3} = \left(\frac{2}{\pi}\right)^3 B_0 \int_0^\infty dx\, x^2 \left[X_{\ell_1}(x) X_{\ell_2}(x) Z_{\ell_3}(x) + X_{\ell_1}(x) X_{\ell_3}(x) Z_{\ell_2}(x) + \right.$$
$$\left. + X_{\ell_3}(x) X_{\ell_2}(x) Z_{\ell_1}(x)\right] . \tag{25}$$

Numerical calculations

- The integrals over k, $X_\ell(x)$ and $Z_\ell(x)$ peak at $x = t_0 - t_{\rm dec}$.

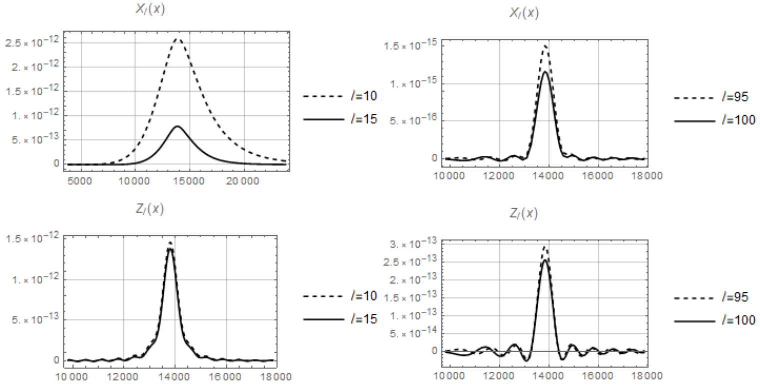

Figure 8: PCMD, R. Durrer, N. Pinto-Neto.

- Numerical results for the reduced bispectrum:

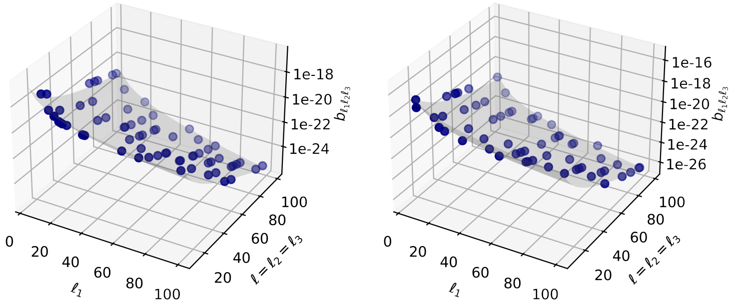

Figure 9: PCMD, R. Durrer, N. Pinto-Neto.

- The local bispectrum:

$$b^{(\mathrm{local})}_{\ell_1\ell_2\ell_3} = \frac{3f_{\mathrm{nl}}(2\pi^2 A_s)^2}{4\times 5^4}\left(\frac{1}{\ell_1(\ell_1+1)\ell_2(\ell_2+1)} + \frac{1}{\ell_1(\ell_1+1)\ell_3(\ell_3+1)} + \frac{1}{\ell_2(\ell_2+1)\ell_3(\ell_3+1)}\right), \qquad (26)$$

- Comparison between the bispectrum of the present model and the local bispectrum: ($\ell_1 = 4$, $\ell_2 = \ell_3 = \ell$, $f_{\mathrm{nl}}(local) = 5.0$):

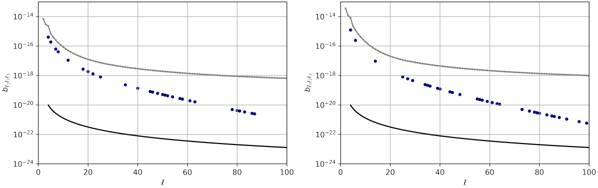

Figure 10: PCMD, R. Durrer, N. Pinto-Neto.

Cosmic variance

- Estimator for the bispectrum:

$$\hat{B}_{\ell_1\ell_2\ell_3} = \sum_{m_1 m_2 m_3} \begin{pmatrix} \ell_1 & \ell_2 & \ell_3 \\ m_1 & m_2 & m_3 \end{pmatrix} a_{\ell_1 m_1} a_{\ell_2 m_2} a_{\ell_2 m_3} . \tag{27}$$

- Its variance reads

$$\mathrm{var}(B_{\ell_1\ell_2\ell_3}) = \langle \hat{B}^2_{\ell_1\ell_2\ell_3} \rangle \simeq C_{\ell_1} C_{\ell_2} C_{\ell_3} \left(1 + \delta_{\ell_1\ell_2} + \delta_{\ell_1\ell_3} + \delta_{\ell_3\ell_2} + 2\delta_{\ell_1\ell_2}\delta_{\ell_2\ell_3}\right) . \tag{28}$$

- For the reduced bispectrum this yields

$$\mathrm{var}\left(b_{\ell_1\ell_2\ell_3}\right) \simeq g^{-2}_{\ell_1\ell_2\ell_3} C_{\ell_1} C_{\ell_2} C_{\ell_3} \left(1 + \delta_{\ell_1\ell_2} + \delta_{\ell_1\ell_3} + \delta_{\ell_3\ell_2} + 2\delta_{\ell_1\ell_2}\delta_{\ell_2\ell_3}\right) . \tag{29}$$

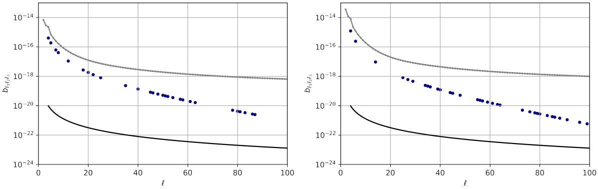

Figure 11: PCMD, R. Durrer, N. Pinto-Neto.

Signal-to-noise ratio

- The SNR is given by

$$\left(\frac{S}{N}\right)^2(\ell_{\max}) = \sum_{\ell_1\ell_2\ell_3=2}^{\ell_{\max}} \frac{b^2_{\ell_1\ell_2\ell_3}}{\mathrm{var}\left(b_{\ell_1\ell_2\ell_3}\right)} \,. \tag{30}$$

- For this computation we use the fits to the reduced bispectrum:

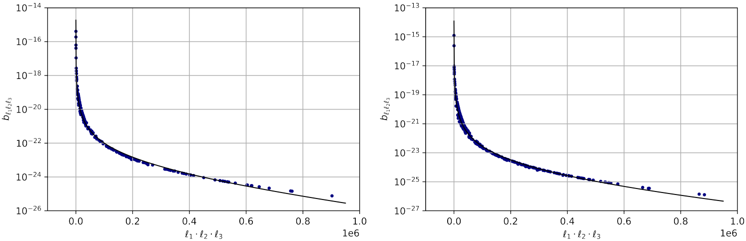

Figure 12: PCMD, R. Durrer, N. Pinto-Neto.

- The SNR, considering a 70% of sky coverage, is

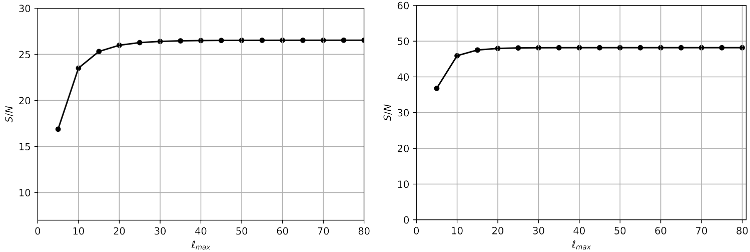

Figure 13: PCMD, R. Durrer, N. Pinto-Neto.

- In all cases of interest, the bispectrum should be detectable in the Planck data.

Overlap with standard bispectrum shapes

- The overlap can be obtained via a scalar product

$$\langle S_1, S_2 \rangle = \int_V S_1(k_1, k_2, k_3) S_2(k_1, k_2, k_3) w(k_1, k_2, k_3) dk_1 dk_2 dk_3, \tag{31}$$

 the weight function $w(k_1, k_2, k_3)$ is an arbitrary non-negative function.

- The projection of the bounce bispectrum in the standard shapes' bispectra is very small:

$$\begin{aligned} \cos\theta^{(\text{bounce,local})} &= 2.369 \times 10^{-4}, \\ \cos\theta^{(\text{bounce,equi})} &= 2.364 \times 10^{-4}, \\ \cos\theta^{(\text{bounce,ortho})} &= -3.985 \times 10^{-5} \end{aligned}$$

for $n = 1/6$

$$\begin{aligned} \cos\theta^{(\text{bounce,local})} &= 7.117 \times 10^{-5}, \\ \cos\theta^{(\text{bounce,equi})} &= 7.071 \times 10^{-5}, \\ \cos\theta^{(\text{bounce,ortho})} &= -1.206 \times 10^{-5} \end{aligned}$$

for $n = 0.21$

Conclusions

- In all cases with sufficient non-Gaussianity to mitigate the large scale anomalies of CMB data, the bispectrum should be detectable in the Planck data.
- The largest contributions to the SNR come from triples (ℓ_1, ℓ_2, ℓ_3) where at least one multipole is smaller than 4, for which the signal is larger than or comparable to the square root of the variance.
- Adding polarisation data may enhance the SNR by about a factor of two.
- These findings motivate us to perform a search for this bispectrum in the actual Planck data.